High-Asymmetry Bipolar Membrane Electrode Assemblies Generate a Superconcentration of Cations and Hydroxide at a Catalyst Surface

Authors: Qiu-Cheng Chen[1]†, Wenjin Zhu[1]†, Yiqing Chen[1]†, Hongmin An[1, 3], Shuang Yang[1], Yong Wang[1], Yali Ji[1], Guangcan Su[1], Rui Wang[1], Jianan Erick Huang[1], Ji-Yoon Song[1], Jaerim Kim[1], Weiyan Ni[1], Charles Musgrave[1], Ke Xie[1]*, Edward H. Sargent[1, 2]*

Affiliations:

[1]Department of Chemistry, Northwestern University, Evanston, IL, USA

[2]Department of Electrical and Computer Engineering, Northwestern University, Evanston, IL, USA

[3]Department of Chemical and Biomolecular Engineering, Korea Advanced Institute of Science and Technology, Daejeon, Republic of Korea

†These authors contributed equally
*Corresponding author. Email: ted.sargent@northwestern.edu; ke-xie@northwestern.edu

Supplementary Notes

Supplementary Note 1 | measurement of D_{K+}

Electrochemical measurements were performed using a standard setup, as described in the Method. During electrolysis, the gas outlet from the MEA was connected to 2 mL of water. After the electrolysis process, the CO gas inlet was disconnected, and a total of 1 mL of water was injected in several portions through the gas inlet to rinse the cathodic chamber. The CO gas was then reconnected to the MEA to facilitate the collection of the rinsing solution. The total volume of the collected solution was determined using a graduated cylinder. The potassium concentration was measured by ICP, and the potassium transport rate was subsequently calculated from the reaction time.

Supplementary Note 2 | COMSOL study

The finite element analysis simulations are performed with the COMSOL Multiphysics software. The FEA model in shown below was defined by the law of mass conservation and electroneutrality assumption of related ions without considering the possible side reactions. Simulation considers the influence of two different factors on ion concentration: concentration diffusion and electric field migration. The simulation model uses a 1D model, which includes the following parts from left to right: Bulk domain (50um thick), Anode domain (200nm thick), cation exchange membrane (CEM, 2~50um thick), anion exchange membrane (AEM, 50um), Cathode domain (200nm). In the simulation model, by adjusting the thickness of CEM through parameterization, different ion concentration distributions can be obtained.

Ohm's law was used to solve the potential profiles in the system, which are necessary for ion electromigration. The equations employed are:

$$\nabla \cdot i_k = 0$$

$$i_k = -\sigma_k \nabla \varphi_k$$

where k is either the electrolyte phase, l, or the solid phase, s, i_k is the current density, σ_k is the conductivity, and φ_k is the potential.

Using the current distribution and concentration diffusion equation to track the current and concentration distribution, the flux of each ion in the electrolyte can be calculated by Nernst-Planck equation,

$$N_i = -D_i \left(\nabla c_i + \frac{F}{RT} z_i c_i \nabla \emptyset_l \right), i = 1, 2, \ldots, n$$

Where D_i, N_i, c_i, z_i, F, T, R, and ϕ_l denote the diffusion coefficient, the flux, the concentration, the charge number, the Faradaic constant, temperature, gas constant, and electrolyte potential, respectively. l stands for the position along the diffusion region of thickness d ($0 < l < d$). Based on the steady-state continuity equations and the law of mass conservation, we have

$$\frac{\partial c_i}{\partial t} + \nabla \cdot N_i = 0$$

and the electroneutrality assumption was represented as

$$F \sum_{i=1}^{n} z_i c_i = 0$$

The boundary condition was set as follows:

$\vec{n} \cdot J = 0$

where J means the ions flux.

The simulation steps include a current distribution initialization and a transient step. Initial K ion concentration of 1800 mol/m^3 and initial OH^- ion concentration of 4200mol/m^3 are set in the Bulk domain, Anode domain, and CEM domain. The potential difference within the electrolyte is set to 0.066V-0.135V.

Supplementary Note 3 | measurement of $pH_{CL/M}$

Preparation of Pt Microelectrode: A homemade platinum disc microelectrode was fabricated using a platinum wire (99.997%, 0.25 mm diameter, Fisher) and a glass capillary (0.5 mm O.D., Fisher). Under a high-temperature flame, the glass melted gently and coated on the Pt wire with the 0.25 mm diameter flat opening.[1-2] The Pt electrode was polished before each experiment.

Preparation of Ag/AgCl reference microelectrode: The electrolyte reservoir was constructed from a glass capillary (0.5 mm O.D., Fisher) sealed with a homemade glass frit. AgCl was electrochemically deposited onto a silver wire (99.95%, 0.203 mm diameter, Fisher) in a solution of 3 M KCl and 0.1 M HCl. Deposition was performed at 5 V for 1 min, followed by10 V for 10 min, using a platinum wire as the counter electrode.[1] The AgCl-coated silver wire and KCl solution were assembled into the electrolyte reservoir, which was then sealed to prevent leakage.

Electrochemical measurements: In addition to the standard MEA cell, two holes (0.5 mm O.D.) were made in the cathode chamber to accommodate the Pt microelectrode and Ag/AgCl reference microelectrode. The distance between the electrode tips and the MEA plane was carefully controlled and fixed between experiments, corresponding to the thickness of the CuNP-coated GDE. The electrodes were secured and fixed using hot glue on the outer side of the chamber.

For pH measurements, a CuNP-coated GDE was prepared by creating two holes in the carbon paper—matching the spacing in the modified cathode chamber—before spray coating. The modified cathode chamber was used in place of the standard cathode chamber during electrolysis and was connected to a potentiostat, as shown in Figure S7. Electrolysis conducted with the modified MEA cell exhibited comparable full-cell voltage and product distribution to the standard MEA cell, suggesting that the internal environment remained representative. Cyclic voltammetry (CV) measurements using the Pt microelectrode were performed immediately after electrolysis via BioLogic program, and resistance-corrected potentials were used to estimate the pH at the membrane-electrode interface. The calibration curve was derived by recording CVs in solutions of different pH, varied by changing the concentration of KOH (Figure S6).[3]

Supplementary Note 4 | Nomenclature and abbreviation[4-5]

In this work, two types of BPM were employed: a homemade forward-bias bipolar membrane, denoted by the nomenclature f-BPM, within which the cation exchange material and anion exchange material were denoted as cation exchange layer (CEL) and anion exchange layer (AEL) respectively; a homemade reverse-bias bipolar membrane, denoted by the nomenclature r-BPM, within which the cation exchange material and anion exchange material were denoted as cation exchange layer (CEL) and anion exchange layer (AEL) respectively. When the cation exchange material is used solely as an membrane, we denoted it as an cation exchange membrane (CEM). When the anion exchange material is used solely as an membrane, we denoted it as an ainion exchange membrane (AEM). For the overall MEA system, we use the abbreviation CEMEA to denote the MEA system with CEM as the ion-exchange membrane; AEMEA to denote the MEA system with AEM as the ion-exchange membrane; f-BPMEA to denote the MEA system with f-BPM as the ion-exchange membrane; r-BPMEA to denote the MEA system with r-BPM as the ion-exchange membrane.

Supplementary Note 5 | Separation cost

In this study, we simulated the separation of ethanol and water through a two-stage distillation process. The model was established in ASPEN Plus V14 using the NRTL method to distillate ethanol to 99.5 wt%. The energy consumption for the separation was evaluated based on the ASPEN Plus Energy Analyzer. The first column removes most of the water, producing a distillate rich in ethanol, while the second column further refines the ethanol to achieve the desired purity. This two-stage distillation configuration effectively represents the industrial rectification process for high-purity ethanol production. The concentration of ethanol in f-BPMEA, AEMEA and CEMEA were 4.8, 3.3, and 1.6 wt% respectively. Distillation cost for f-BPMEA, AEMEA and CEMEA was estimated to be 400, 487 and 893 USD/t.

Supplementary Note 6 | Discussion of degradation of f-BPMEA

The stable operation of our system is currently limited to 28 hours, a bottleneck governed by the integrated system design and attributable to the durability of the membrane and copper catalyst. The operational principle, which relies on generating an extreme local alkaline environment and high product concentration, creates a highly aggressive cathodic environment. We hypothesize this environment induces two primary degradation pathways: (1) Reconstruction of the Cu catalyst, driven by a synergistic effect of high alkalinity[6] and cations[7]. (2) Chemical degradation of the anion exchange membrane via nucleophilic attack by OH^- or swelling by alcohol.[8] This fundamental trade-off between high product yield and long-term component stability is a central insight of our work. Consequently, developing components with enhanced resilience to these extreme conditions constitutes the critical next step and the immediate focus of our ongoing research.

Supplementary Figures

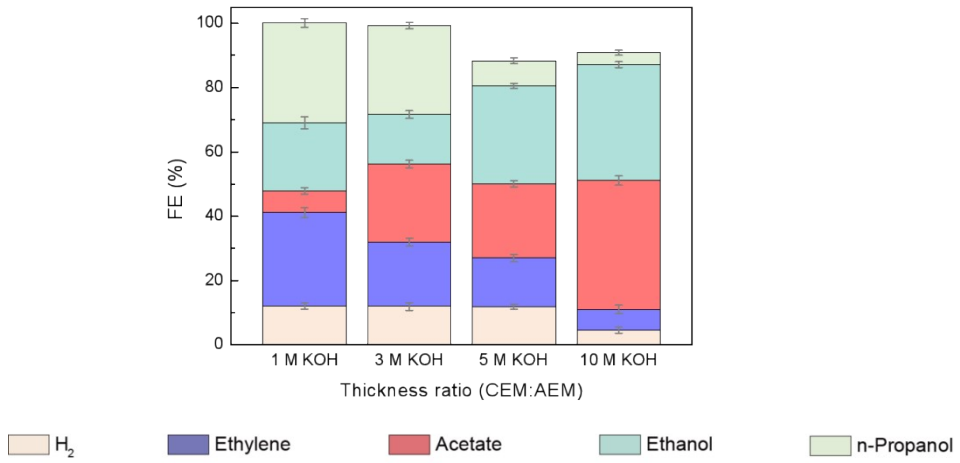

Figure S1. Faradaic efficiency profiles for CO reduction on Cu catalyst using AEMEA at -100 mA cm^{-2} with 1, 3, 5, 10 M KOH anolyte.

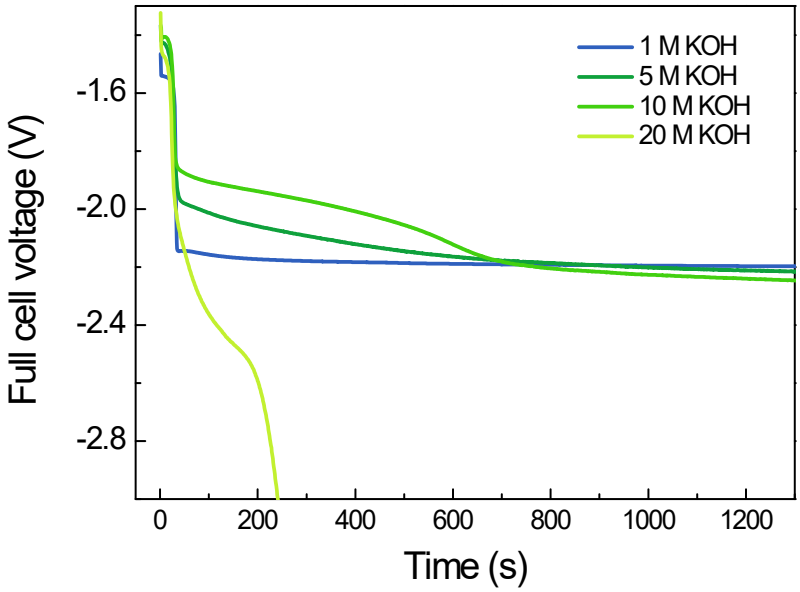

Figure S2. Cell voltage for CO reduction in AEMEA at -100 mA cm^{-2} with 1, 5, 10, 20 M KOH anolyte.

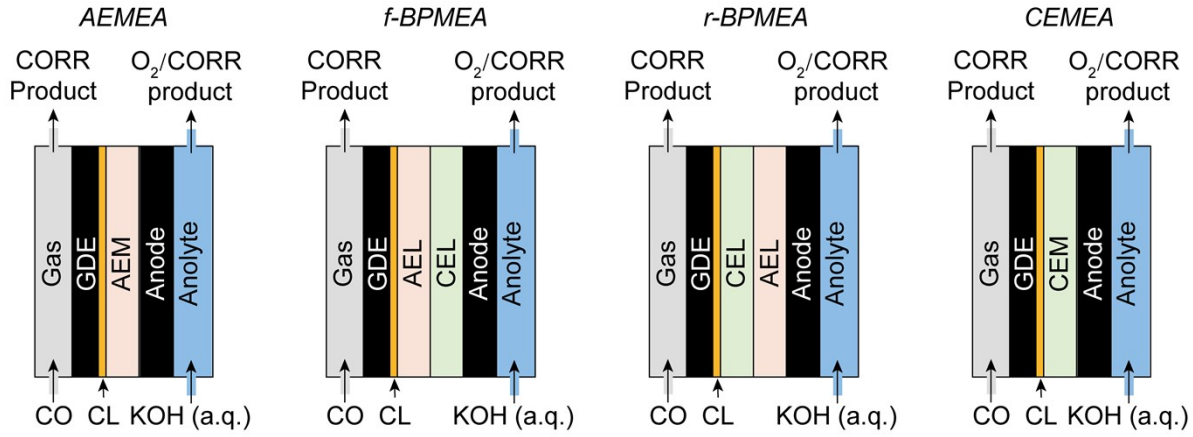

Figure S3. Scheme for MEA and picture for MEA with different membrane confrontations.

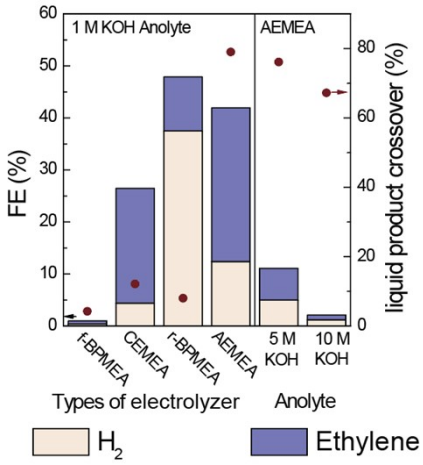

Figure S4. Faradaic efficiency of gas CORR liquid products in MEA with different membrane or anolyte.

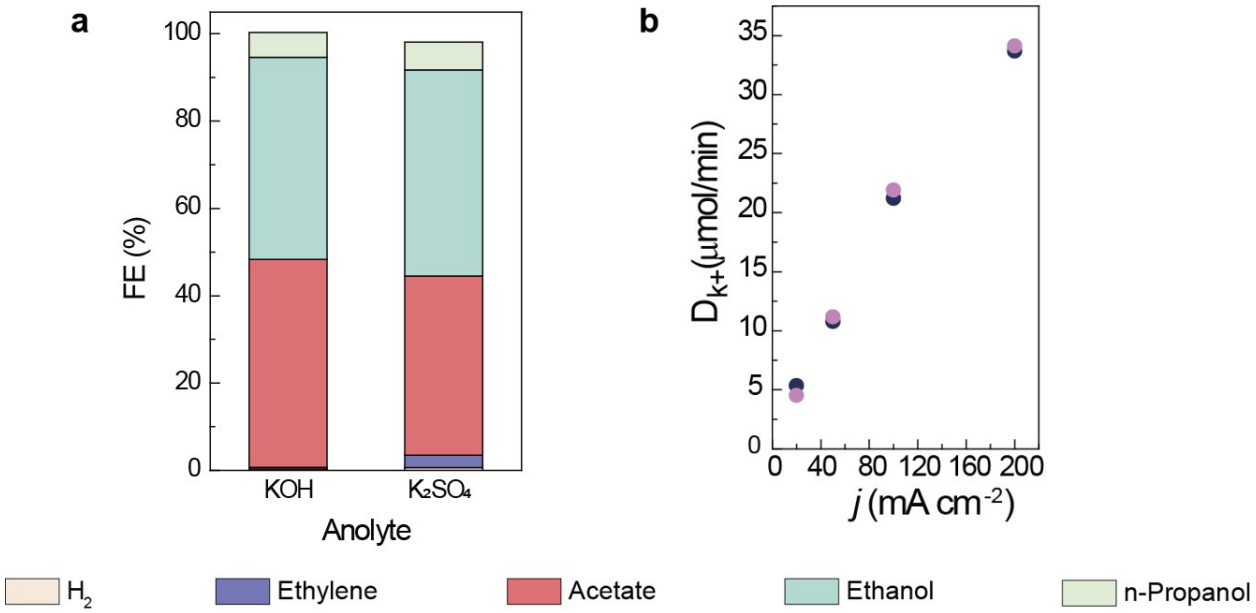

Figure S5. Faradaic efficiency of CORR liquid products and D_{K+} in f-BPMEA with 1 M KOH and 0.5 M K_2SO_4.

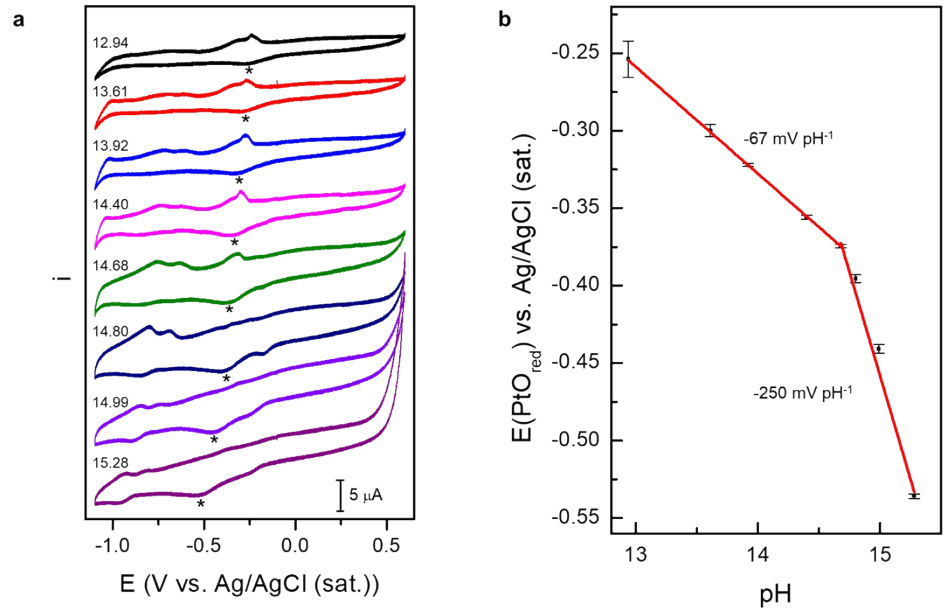

Figure S6. a) pH-dependent CVs obtained using Pt nanoelectrode (ø = 250 nm) in KOH solutions with pH from 12.94 to 15.28. CVs (scan rate: 100 mV s^{-1}) were acquired between +600 and −1100 mV vs. Ag/AgCl. b) Calibration curves derived from the $PtO_{red.}$ peak position (E_{PtOred}) as a function of the pH values. Linear fits (red lines) with different slopes (displayed in mV pH^{-1}) suggest distinct pH dependencies between 12.94 and 14.68 mol L^{-1} and between 14.68 and 15.28 pH values as suggested by the slopes of −67 mV pH^{-1} and −250 mV pH^{-1}, respectively. Peak positions are averaged over 3 different calibration measurements.

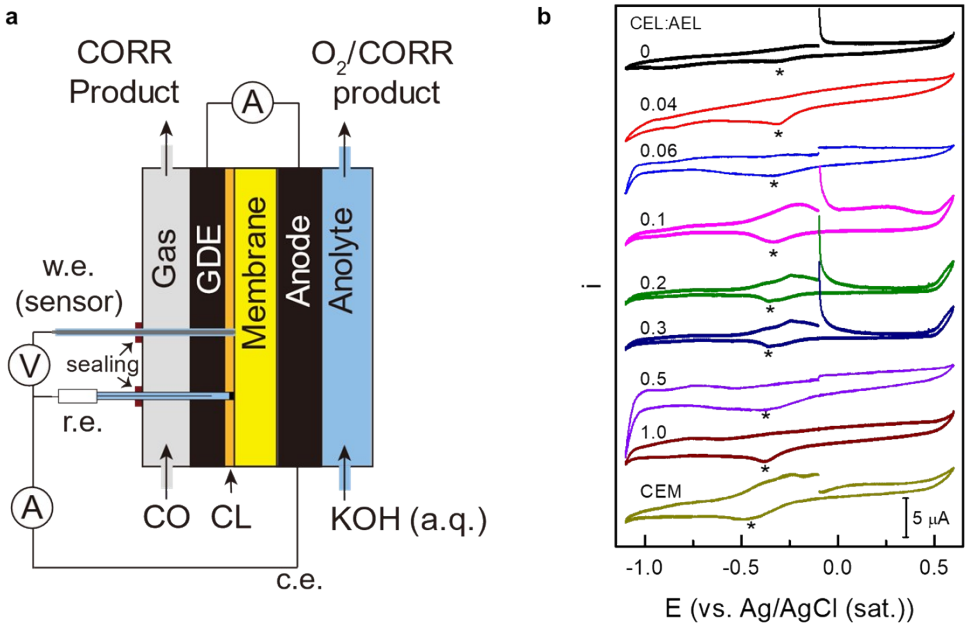

Figure S7. Setup for pH measurements

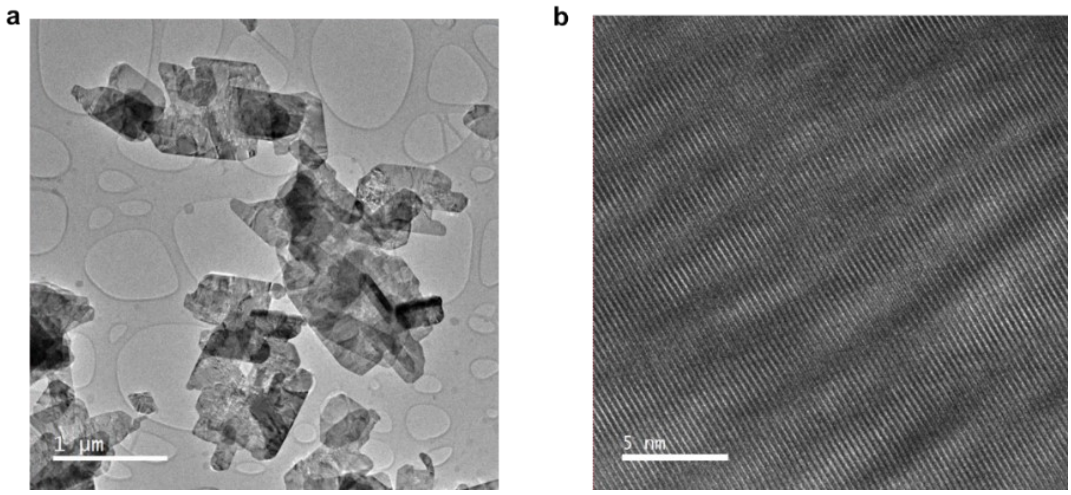

Figure S8. TEM and HRTEM images of CuO pre-catalysts.

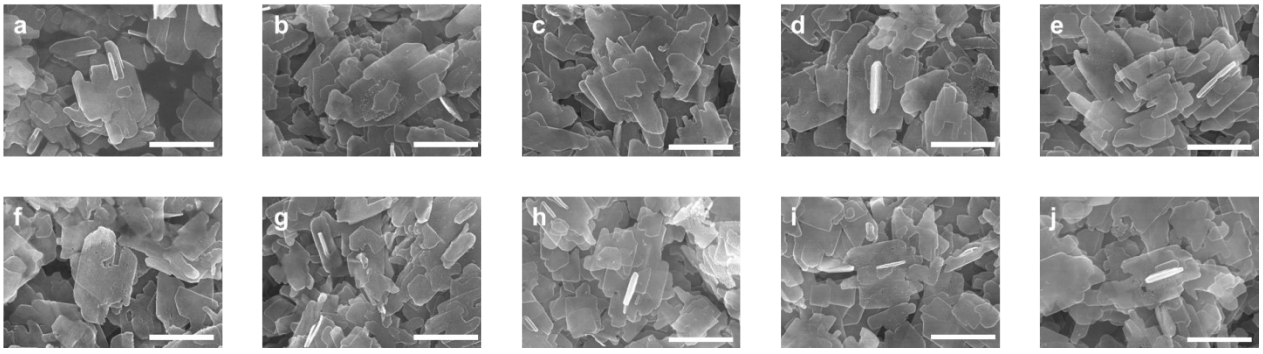

Figure S9. Scanning electron microscopic (SEM) image of the CuNP-coated electrode before (a) and after electrolysis with CEL-to-AEL ratio from 0 to 1 (b-i) as well as CEM (j). The bar represents 1 µm distance.

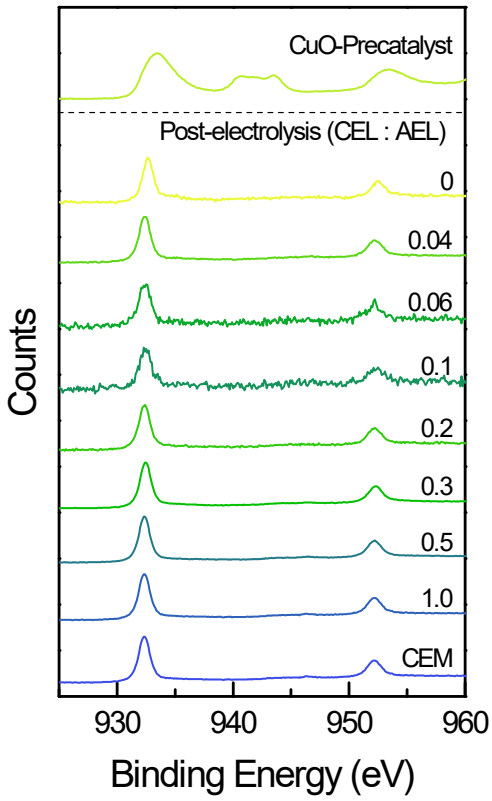

Figure S10. high-resolution XPS spectra of Cu/CuO GDE before and after electrolysis in different MEA systems.

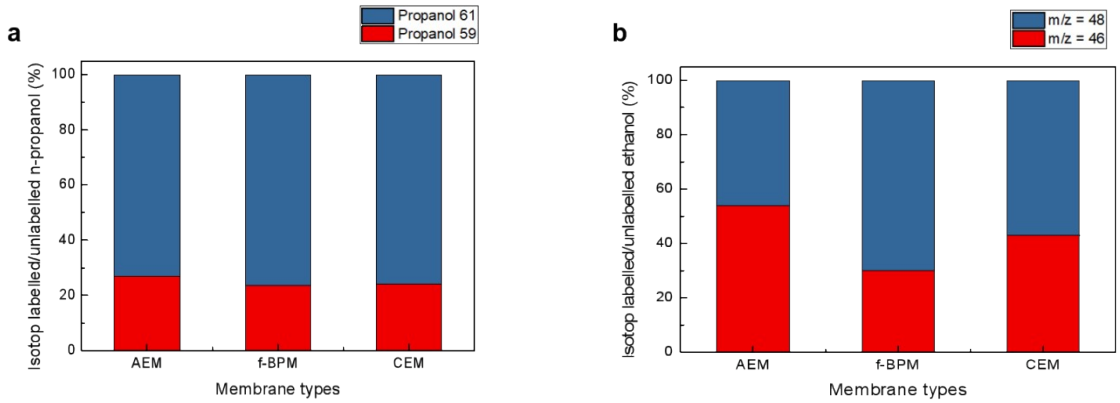

Figure S11. Isotop labelled (blue) and unlabelled (red) n-propanol (a) and ethanol (b) from CORR with different membranes in MEA system quantified from EC-MS measurements.

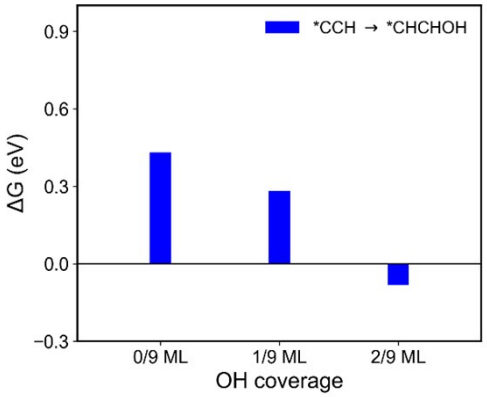

Figure S12. The reaction energies for the *CCH→*CHCHOH step at various OH coverage.

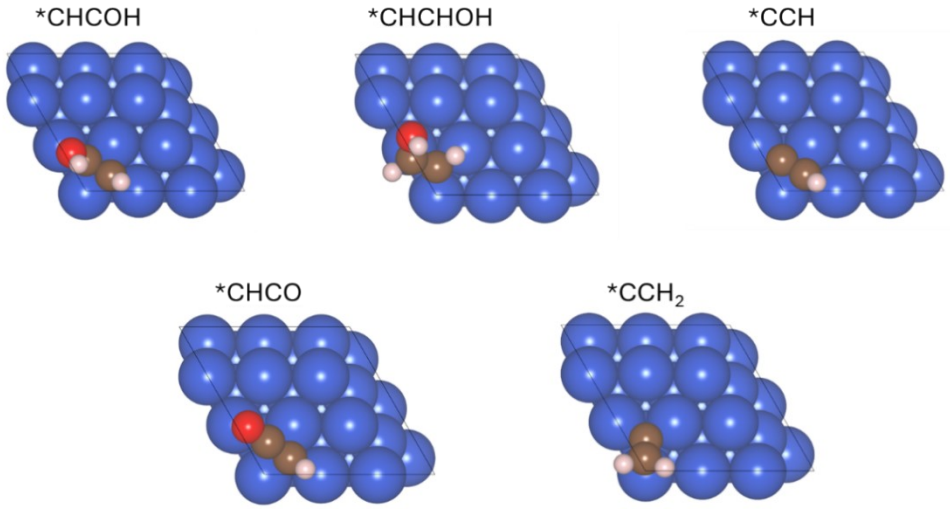

Fig. S13 Optimized adsorption configurations of reaction intermediates on Cu(111) at 0/9 ML OH coverage. Water layers are not shown for clarity.

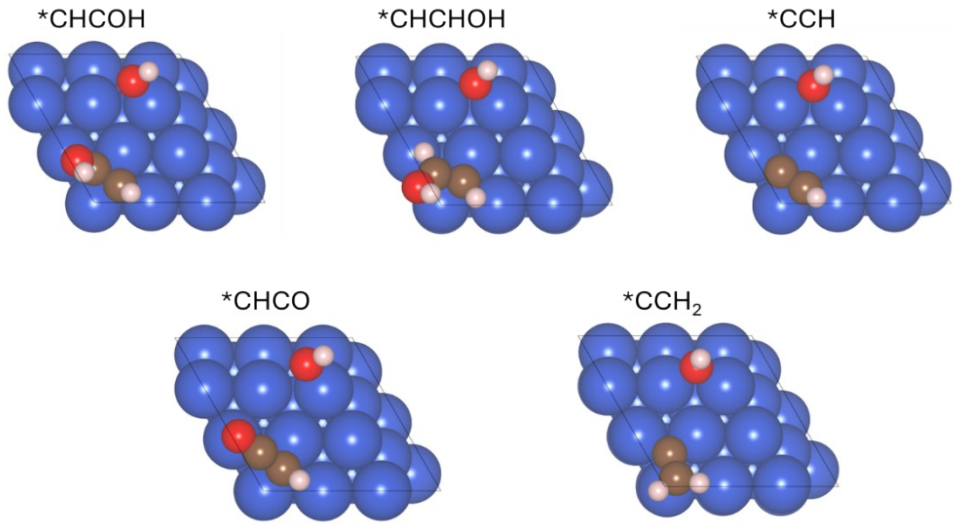

Fig. S14 Optimized adsorption configurations of reaction intermediates on Cu(111) at 1/9 ML OH coverage. Water layers are not shown for clarity.

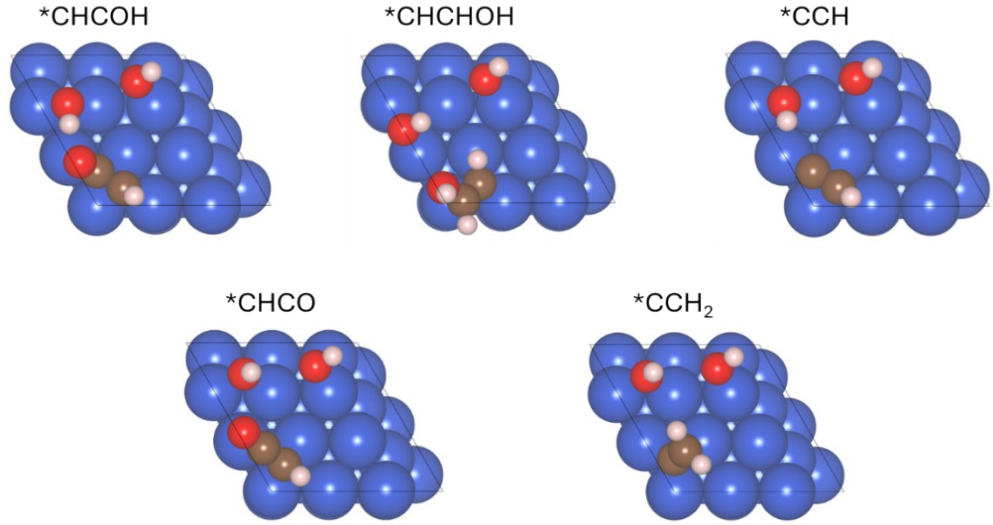

Fig. S15 Optimized adsorption configurations of reaction intermediates on Cu(111) at 1/9 ML OH coverage. Water layers are not shown for clarity.

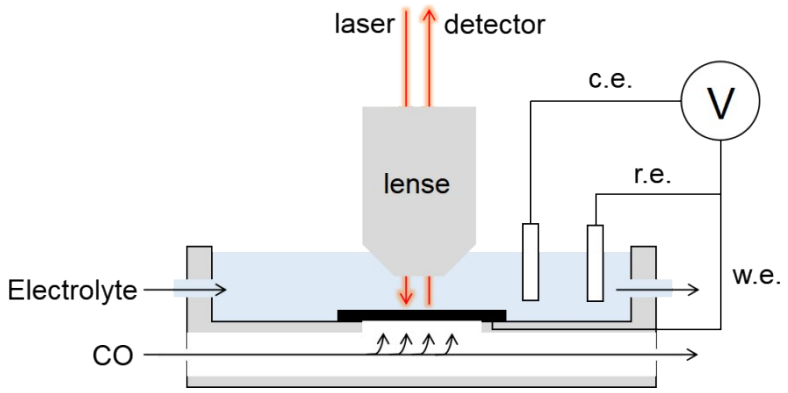

Fig. S16 Scheme of Raman configuration.

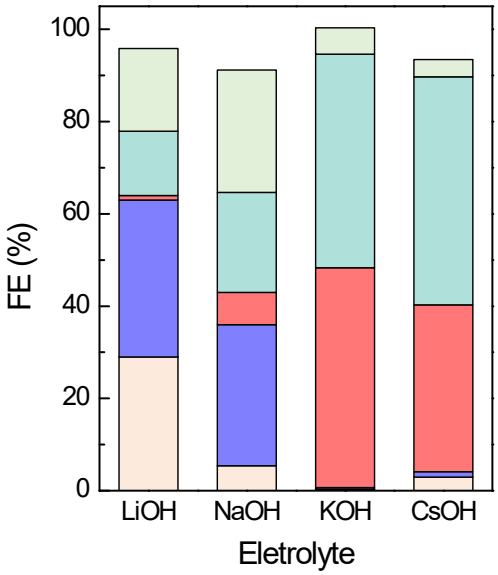

Fig. S17 Faradaic efficiency profiles for CO reduction on Cu catalyst using f-BPMEA at -100 mA cm^{-2} with 1 M LiOH, NaOH, KOH, CsOH anolyte.

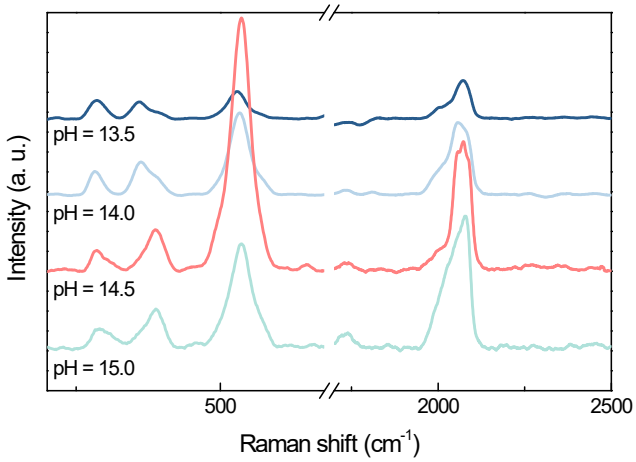

Fig. S18 Operando Raman spectra of CuNPs acquired during CORR at bulk pH 13.5-15.0 at potential equal to -0.4 V vs. RHE.

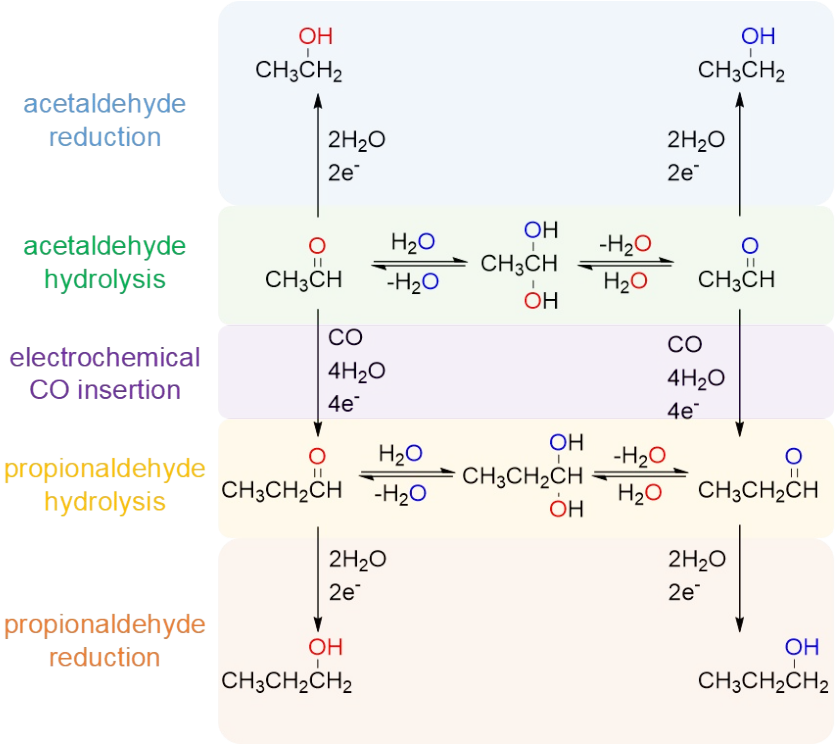

Fig. S19 Proposed aldehyde pathway for alcohol production, with oxygen in different colors to indicate the exchange of O atoms. Notes: Other than the *CCH intermediate for ethanol production, acetaldehyde was also widely consider as intermediate to generate ethanol after electrochmeical reduciton.[9-10] Under this route, the acetaldehyde intermediate are likely to undergo rapid and reversible hydrolysis step, and simultaneously exchange the O atom between aldehyde and bulk water.[11]

Supplementary Tables

Table S1. Product FEs and full cell votages of CORR in different f-BPMEAs .

		Faraday Efficiency (%)					
Thickness ratio (CEL:AEL)	Full cell voltage (V)	n-Propanol	Ethanol	Acetate	Ethylene	Hydrogen	Total
0 (AEM)	-2.11	31.02	21.17	6.75	29.04	12.1	100.08
0.04	-2.14	30.37	24.68	8.65	28.05	8.24	99.99
0.06	-2.14	26.93	29.31	16.85	18.63	4.78	96.5
0.1	-2.15	17.34	38.2	27.3	13.29	0.98	97.11
0.2	-2.16	10.91	37.39	40.7	7.75	1.01	97.76
0.3	-2.17	4.29	38.12	45.59	3.7	0.62	92.32
0.5	-2.17	8.55	43.58	41.45	0.6	0.4	94.58
1	-2.20	3.07	48.09	33.12	6.78	4.76	95.82
CEM	-2.15	5.81	51.45	13.34	22.07	4.4	97.27

Table S2 Performance summary of concentrated C_{2+} liquids production from CORR-MEA

System	**$FE_{ethanol}$**	**FE_{liquid}**	**EE_{c2+}**	**Liquid concentration**	**Stability**	**Ref.**
AEMEA(1M KOH)	30.3%	64.8%	38.6%	18.8 wt%	100	JACS 2024[12]
CEMEA (1M NaOH)	10%	31%	-	1.1 M	24	Joule 2019[13]
AEMEA (1M KOH)	15%	61.5%	37%	-	100	Nat. Energy 2022[14]
AEMEA (1M KOH)	20%	62%	-	-	100	Nat. Comm.2023[15]
CEMEA (1M NaOH)	-	-	-	5.5 wt% (acetate)	18	Nat. Synth. 2023[16]
f-BPMEA (1M KOH)	44%	93%	40.5%	23 wt%	28	This work

References

[1] A. Botz, J. Clausmeyer, D. Ohl, T. Tarnev, et al., *Angew. Chem. Int. Ed.* **2018**, *57*, 12285-12289.
[2] S. Dieckhofer, D. Ohl, J. R. C. Junqueira, T. Quast, et al., *Chemistry* **2021**, *27*, 5906-5912.
[3] J. Li, Y. Kuang, X. Zhang, W.-H. Hung, et al., *Nat. Catal.* **2023**, *6*, 1151-1163.
[4] S. Z. Oener, M. J. Foster, S. W. Boettcher, *Science* **2020**, *369*, 1099-1103.

[5] J. C. Bui, E. W. Lees, D. H. Marin, T. N. Stovall, et al., *Nature Chemical Engineering* **2024**, *1*, 45-60.
[6] Q. Liu, Q. Jiang, L. Li, W. Yang, *J. Am. Chem. Soc.* **2024**, *146*, 4242-4251.
[7] S. Liu, Y. Li, D. Wang, S. Xi, et al., *Nat Commun* **2024**, *15*, 6092.
[8] F. Habibzadeh, P. Mardle, N. Zhao, H. D. Riley, et al., *Electrochemical Energy Reviews* **2023**, *6*.
[9] E. Bertheussen, A. Verdaguer-Casadevall, D. Ravasio, J. H. Montoya, et al., *Angew. Chem. Int. Ed.* **2016**, *55*, 1450-1454.
[10] E. L. Clark, A. T. Bell, *J. Am. Chem. Soc.* **2018**, *140*, 7012-7020.
[11] M. Jouny, W. Luc, F. Jiao, *Nat. Catal.* **2018**, *1*, 748-755.
[12] G. Zhou, B. Li, G. Cheng, C. J. Breckner, et al., *Journal of the American Chemical Society* **2024**, *146*, 31788-31798.
[13] D. S. Ripatti, T. R. Veltman, M. W. Kanan, *Joule* **2019**, *3*, 240-256.
[14] X. Wang, P. Ou, A. Ozden, S.-F. Hung, et al., *Nat. Energy* **2022**, *7*, 170-176.
[15] W. Niu, Z. Chen, W. Guo, W. Mao, et al., *Nat Commun* **2023**, *14*, 4882.
[16] R. Dorakhan, I. Grigioni, B.-H. Lee, P. Ou, et al., *Nature Synthesis* **2023**, *2*, 448-457.